LAWRENCE
LIVERMORE
NATIONAL
LABORATORY

LLNL-CONF-431874

Thomson-Scattering Measurements in the Collective and Non-collective Regimes in Laser Produced Plasmas

J. S. Ross, S. H. Glenzer, J. P. Palastro, B. B. Pollock, D. Price, G. R. Tynan, D. H. Froula

May 14, 2010

18th Topical Conference High Temperature Plasma Diagnostic
Wildwood , NJ, United States
May 16, 2010 through May 20, 2010

Disclaimer

Thomson-scattering measurements in the collective and non-collective regimes in laser produced plasmas

J. S. Ross[1,2], S. H. Glenzer[1], J. P. Palastro[3], B. B. Pollock[1,2], D. Price[1], G. R. Tynan[2], and D. H. Froula[1]

[1] *Lawrence Livermore National Laboratory, University of California, P.O. Box 808, Livermore, California 94551*
[2] *Mechanical and Aerospace Engineering Department, University of California at San Diego, 9500 Gilman Drive, La Jolla, CA 92093-0411 and*
[3] *Institute for Research in Electronics and Applied Physics, College Park, Maryland 20740, USA*

We present simultaneous Thomson-scattering measurements of light scattered from ion-acoustic and electron plasma fluctuations in a N_2 gas jet plasma. By varying the plasma density from 1.5×10^{18} cm^{-3} to 5.0×10^{19} cm^{-3} and the temperature from 100 eV to 600 eV we observe the transition from the collective regime to the non-collective regime in the high-frequency Thomson scattering spectrum. These measurements allow an accurate local measurement of fundamental plasma parameters: electron temperature, density and ion temperature. Furthermore, experiments performed in the high-densities typically found in laser produced plasmas results in scattering from electrons moving near the phase velocity of the relativistic plasma waves. Therefore, it is shown that even at low temperatures, relativistic corrections to the scattered power must be included.

PACS numbers:

I. INTRODUCTION

Thomson Scattering is a valuable diagnostic for characterizing laser [1–4], tokamak [5–7] and pinch [8, 9] plasmas. Thomson scattering is the scattering of photons from free electrons when the photon energy is less than the rest mass of an electron. Figure 1 shows a complete scattering spectrum as a function of the scattering parameter, $\alpha \equiv 1/k\lambda_D$. Transitions between collective and non-collective scattering are observed, but typically laser plasmas are limited to the collective regime as a result of the high densities (i.e., associated small λ_D) required for coupling the laser beam energy to the plasma ($n_e \gtrsim 10^{19}$ cm^{-3}).

In the high-frequency regime ($\omega > \omega_{pi}$), the transition to collective scattering is characterized by $\alpha = 1$. When $\alpha > 1$, light is scattered from electron-plasma fluctuations with a wavelength longer than the Debye length ($\lambda_D = \sqrt{kT_e/4\pi n_e e^2}$) and the scattering spectrum revels the corresponding "electron feature". For $\alpha < 1$, light is scattered from electrons inside the Debye sphere and the scattering spectrum resembles the electron distribution function.

Similarly, when observing low-frequency fluctuations ($\omega < \omega_{pi}$), the electrons contributing to the scattering spectrum are associated with screening the ions. When the ion-acoustic waves are weakly damped [$\alpha \gtrsim (ZT_e/3.45T_i - 1)^{-1/2}$], the collective motion associated with the "ion feature" is apparent in the scattering spectrum and, for $\alpha \lesssim (ZT_e/3.45T_i - 1)^{-1/2}$, the spectrum revels the ion distribution function.

When scattering from high-frequency fluctuations in the collective regime, the electron temperature and density can be determined from the width and the frequency of the electron-plasma wave resonance respectively. In the collective low-frequency regime, the frequency of the ion-acoustic features provide a measure of the sound speed $c_s \simeq \sqrt{(ZT_e + 3T_i)/M_i}$. For mid- to high-Z laser-plasmas, $ZT_e >> 3T_i$ and the ion feature typically provides a measure of the electron temperature when the average charge state is known [10, 11]. Conversely, when the electron temperature is known, for example, from simultaneous measurement of the electron feature, then either the average charge state [12] or the ion temperature can be determined.

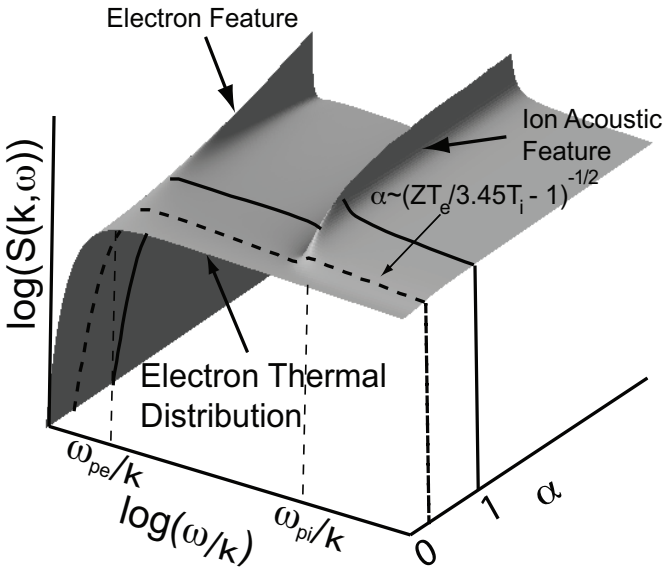

FIG. 1: The Thomson scattering spectrum as a function of the scattering parameter. The charge state (Z=10) and the electron and ion temperatures are held constant ($T_e/T_i = 1$) while the density is varied to change the scattering parameter.

In this study, the electron temperature, density, and ion temperature is characterized in a laser produced gas

jet plasma by simultaneously resolving the electron and ion features. The transition from the non-collective to collective high-frequency regime is observed by scaling the plasma density from 1.5×10^{18} cm^{-3} to 4×10^{19} cm^{-3}. Furthermore, scattering from the high-density plasmas where the electron-plasma fluctuations have relativistic phase velocities demonstrates the need to include relativistic modifications to the Thomson scattering calculations. As the phase velocity is primarily a function of the plasma frequency ($\omega \approx \omega_{pe}$), this effect is independent of the electron temperature and is dominant at high densities which is experimentally demonstrated in a traditionally classical regime ($v_{osc}/c = eE_0/cm\omega_0 << 1$ and $T_e < 1$ keV) [13].

II. EXPERIMENT

The experiments were performed at the Jupiter Laser Facility, Lawrence Livermore National Laboratory using the Janus Laser. The plasmas were produced using a 2ω ($\lambda_i = 2\pi/k_i = 527$nm) laser beam focused with a 1 meter focal length lens ($f/6.7$) about 1 mm from a 1.5 mm diameter cylindrical gas jet nozzle with an operating upstream pressure of 50 to 300 psi. This resulted in initial electron densities from 1.5×10^{18} cm^{-3} to 5.0×10^{19} cm^{-3}. For densities below 2×10^{18} cm^{-3}, helium gas was used; above this density nitrogen gas was used.

The experimental geometry is shown in Figure 2. Two laser beam configurations were used to study the hydrodynamics of the gas jet plasmas. Configuration A employed a 100 J, 1-ns long square pulse followed 4 ns later by a 20 J, 200-ps long Gaussian pulse. A continuous phase plate (CPP) [14] was used to produce a 200 μm diameter laser spot at the center of the gas jet. A second 2ω, 2 J, 4-ns long laser beam probed the plasma condition when the primary beam was off. This beam was focused with a 40 cm long focal length lens ($f/10$) which produced a 70 μm diameter spot which over-lapped the primary beam at best focus. Configuration B employed a single 300 J, 3-ns long square pulse laser beam that was focused with a 600 μm diameter phase plate.

Two Thomson scattering diagnostics are configured to simultaneously measure the high- and low-frequency components of the scattered spectrum. An $f/4$ lens collects the light scattered 90° relative to both the primary and probe beams. To maximize the scattered signal, both laser beams are polarized in the plane perpendicular to the collection lens. The collected light is collimated and transported out of the vacuum. A 527 nm notch filter is used slightly off normal to reflect the low-frequency scattered light.

The light reflected from the notch filter is collected and focused by an $f/10$ lens to the 100 μm slit of a 1-meter image spectrometer which is coupled to a Hamamatsu 7700 streak camera. Using a 1200 grooves/mm grating in second order and a 200 μm streak camera entrance slit results in a spectral resolution of $\delta\lambda = 0.23$ nm and a temporal resolution of $\delta t = 400$ ps [15].

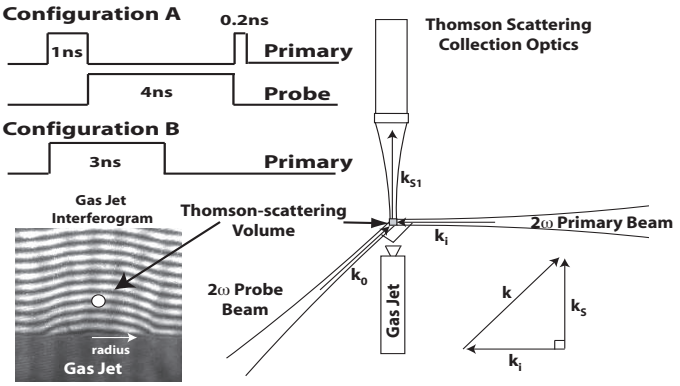

FIG. 2: The experimental setup is shown. The 2ω primary beam is normal to the direction of scattered light collection and define a plane. The 2ω probe beam is normal to that plane. The beam timing configurations, a sample gas jet interferogram, and the Thomson scattering k-vector diagram are shown.

The light transmitted through the notch filter is focused by an $f/5$ mirror onto the 50 μm entrance slit of a 1/3-meter imaging spectrometer which is coupled to a Hamamatsu 7700 streak camera. A 150 grooves/mm grating is used with a resulting spectral resolution of $\delta\lambda = 1.6$ nm. The spectral resolution of both systems is measured using the 546 nm line from a Hg calibration lamp. A 200 μm streak camera entrance slit resulted in a temporal resolution of $\delta t \simeq 100$ ps. The Thomson scattering volume is defined for both systems by the overlapping slits with the laser beams.

Two streak tubes (S1 and S20) were tested to optimize the quantum efficiency on the high-frequency Thomson scattering diagnostic. Figure 3 shows the resulting sensitivities of the systems over the wavelength region of interest. The spectral response of the complete Thomson scattering system was measured by placing the output of a calibrated tungsten lamp at the Thomson scattering volume. By dividing the known tungsten spectrum by the measured spectrum a calibration factor is found which is shown in Figure 3. The S1 streak tube was chosen for measurements where the intensity between the two electron plasma features was being compared. This correction is critical for comparing the intensity of the Thomson-scattering peaks which can be separated by over 100 nm.

III. THOMSON SCATTERING

The scattered power into a unit solid angle $d\Omega$ and a unit frequency $d\omega$ is given by [16],

$$P(\mathbf{R},\omega_s)d\Omega d\omega_s = \frac{P_i r_0^2}{A} d\Omega \frac{d\omega_s}{2\pi} N S(\mathbf{k},\omega) G(\mathbf{k},\omega), \quad (1)$$

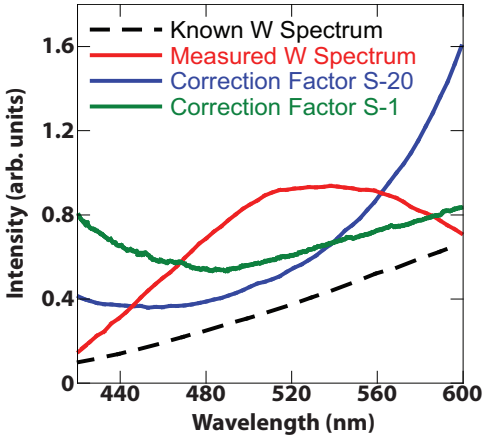

FIG. 3: The 1/3-meter spectrometer coupled to a streak camera is calibrated for wavelength sensitivity using a tungsten lamp. The measured spectrum for an S-20 streak tube is shown (red curve). The ratio of the known spectrum (black dashed line) to the measured spectrum (red line) results in the correction factor. Two correction factors are shown, one for the S-1 (green line) streak tube and one for the S-20 (blue line) streak tube.

where P_i is the incident power, A is the cross-sectional area of the Thomson-scattering volume, r_0 is the classical electron radius, N is the electron density, $S(\mathbf{k},\omega)$ is the spectral density function, and $G(\mathbf{k},\omega)$ is a geometrical factor.

The Thomson-scattering spectral density function accounts for the motion of the plasma and is expressed as,

$$S(\mathbf{k},\omega) = \frac{2\pi}{k}\left|1-\frac{\chi_e}{\varepsilon}\right|^2 f_{e0}\left(\frac{\omega}{k}\right) + \frac{2\pi Z}{k}\left|\frac{\chi_e}{\varepsilon}\right|^2 f_{i0}\left(\frac{\omega}{k}\right), \tag{2}$$

where $\varepsilon = 1+\chi_e+\chi_i$ is the dielectric function, χ_e is the electron susceptibility, χ_i is the ion susceptibility, Z is the average ionization state, $\omega = \omega_s - \omega_i$, ω_s is the scattered frequency, ω_i is the incident frequency and $f_{e0}(\frac{\omega}{k})$ and $f_{i0}(\frac{\omega}{k})$ are the distributions for electrons and ions respectively.

The geometrical factor [16] accounts for the electromagnetic interactions with the plasma. The geometric factor becomes unity in the "non-relativistic" limit (i.e., using a zero order in (v/c) calculation) and assuming collection of the scattered light normal to the direction of the laser beam polorization ($|\hat{k}_s\times(\hat{k}_s\times\hat{E}_i)|^2 = 1$). When ignoring terms of order $(v/c)^2$ and greater the geometrical factor becomes,

$$G(\mathbf{k},\omega) = \left(1+\frac{2\omega}{\omega_i}\right). \tag{3}$$

In this limit the geometric factor results in an asymmetric scattering spectrum which is attributed to two effects which can be expressed as the ratio of peak values,

$$\frac{P^{blue}}{P^{red}} \approx \underbrace{\frac{P^{blue}_{NR}}{P^{red}_{NR}}}_{A}\underbrace{\left(\frac{1+\beta\cos\phi}{1-\beta\cos\phi}\right)^2}_{B}\underbrace{\left(\frac{1+\beta\cos\Phi}{1-\beta\cos\Phi}\right)^2}_{C} \tag{4}$$

where the electrons contributing to the peak scattered power are moving near the phase velocity of the fluctuation $\beta \equiv \omega/kc$. Here, ϕ is the angle between $\hat{k}$ and $\hat{k}_s$, Φ is the angle between $\hat{k}$ and $\hat{k}_i$. Term A is the ratio of the peak powers in the blue- and red-shifted peaks respectively calculated for the "non-relativistic" geometric factor, i.e., $G(k,\omega) = 1$. Asymmetries associated with Term A are a result of the difference in magnitude between the red- and blue-shifted resonant wave vectors which is approximately $2\sqrt{\frac{n_e}{n_c}} > 10\%$. When the Landau damping is small, modest differences in the plasma wave vector result in large relative changes in the damping of the plasmas waves.

Term B is a result of the relativistic aberration of light, also referred to as the relativistic headlight effect, where light is preferentially directed in the emitters direction of propagation. Term C is an expression that accounts for the electron motion in the direction of the incident light vector E_i interacting with the magnetic field of the Thomson scattering probe laser. The resulting $v\times B_i$ force is in the same direction as the force of the incident electric field. When the electron is moving towards the detector, the increased force on the electron enhances the scattered power. When the electron is moving away from the detector the force is in the opposite direction and the scattered power is reduced. For a $\theta = 90°$ scattering angle, Terms B and C in Eqn. 4 reduce to Eqn. 3 when keeping only terms first order in v/c.

The phase velocity (ω/k) of the plasma wave is calculated from the plasma density, the experimental geometry and the incident laser wavelength. The wave number $(\mathbf{k})$ is given by the incident wave number $(\mathbf{k}_i)$ and the scattered wave number $(\mathbf{k}_s)$ using the law of cosines, $k = \sqrt{|\mathbf{k}_s|^2+|\mathbf{k}_i|^2-|\mathbf{k}_s||\mathbf{k}_i|\cos\theta}$, where θ is the angle between $\mathbf{k}_s$ and $\mathbf{k}_i$. The wave numbers are calculated from their respective frequencies using the dispersion relation for an electromagnetic wave in a plasma, $k_{i,s} = \sqrt{\omega^2_{i,s}-\omega^2_{pe}}/c$. The phase velocity can then be estimated for $\theta = 90°$ by assuming $\omega \approx \omega_{pe}$,

$$\beta \equiv \frac{\omega}{kc} = \left(2\frac{n_c}{n_e} - 1 + 2\sqrt{\frac{n_c}{n_e}}\right)^{-1/2} \tag{5}$$

where n_c is the critical density for the wavelength of the Thomson scattering probe beam.

Figure 4 shows the effect of the relativistic corrections on the scattering spectrum. The measured spectrum is fit using Eqn. 1 using both the relativistic and "non-relativistic" geometric factors and an electron temperature of 410 eV and a density of 4×10^{19} cm^{-3} is determined. These conditions corresponds to a normalized

phase velocity of $\beta = 0.07$. When accounting for the effects of Landau damping, $P_{NR}^{blue}/P_{NR}^{red} = 0.7$, the total asymmetry calculated by Eqn. 4 is $P^{blue}/P^{red} = 1.1$ which compares well to the measured value of 1.2. This result demonstrates the importance of including first order v/c corrections to the calculation of scattered power for nearly all collective scattering from high-frequency fluctuations in laser-produce plasmas.

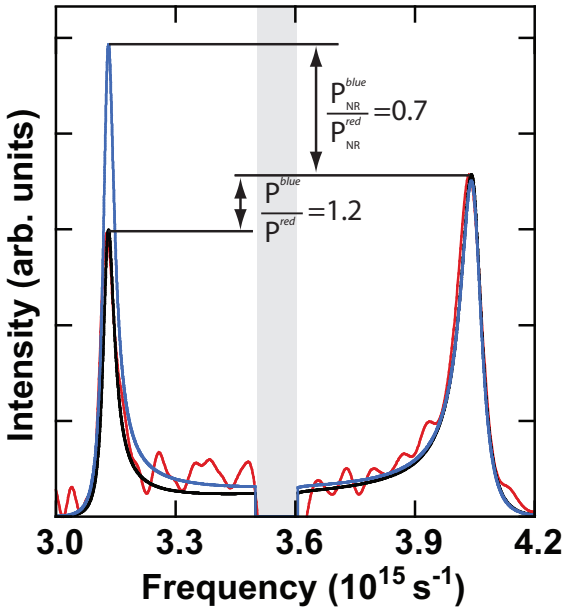

FIG. 4: A measured high-frequency scattering spectrum (red line) is compared to the Thomson scattering form factor using a relativistic (black line) and a "non-relativistic" (blue line) treatment. Both calculations use an electron temperature of 4×10^{19} cm^{-3} and an electron temperature of 410 eV. The scattering parameter for these conditions is $\alpha = 2.5$ and $\beta = 0.7$ from Eqn. 5.

A. Scattering from high-frequency fluctuations

Figure 5 shows scattering from high-frequency fluctuations where the transition from the collective regime ($\alpha > 1$) to the non-collective regime ($\alpha < 1$) is seen. The scattering parameter was varied by changing the initial gas density which resulted in a range of densities and electron temperatures. In the collective regime, the wavelength associated with the peak of the electron feature is primarily a function of the density; a larger density results in an increased separation between the two electron-plasma features ($\Delta\lambda_{EPW}$). The separation can be approximated for $\theta = 90°$ and low densities ($n_e/n_c \lesssim 0.05$) as,

$$\frac{\Delta\lambda_{EPW}}{\lambda_i} \approx 2\left[\frac{n_e}{n_c} + 6\left(\frac{v_{th}}{c}\right)^2\right]^{1/2}\left(1 + \frac{3}{2}\frac{n_e}{n_c}\right) \qquad (6)$$

where λ_i is the incident wavelength and $v_{th} = \sqrt{\kappa_b T_e/m_e}$.

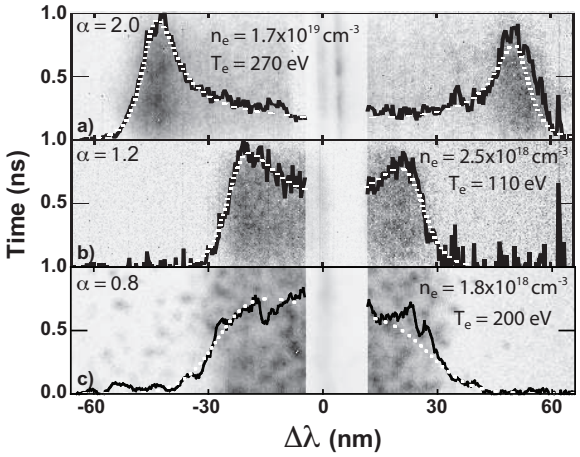

FIG. 5: Three streak camera records of the Thomson scattering spectrum from the electron feature are shown for different plasma conditions. The scattering parameter decreases as the density decreases:(a) 1.7×10^{19} cm^{-3}, (b) 2.5×10^{18} cm^{-3}, (c) 1.8×10^{18} cm^{-3}. The spectra at 0.5 ns in each streak record (black lines) are shown. The calculated Thomson scattering spectrum (dashed-white line) using the temperature and density is plotted for each spectra. The attenuated region at $\delta\lambda = 0$ is due to the 2ω notch filter.

Figure 6(a) shows the sensitivity of the scattering spectrum to the electron density in the collective regime. Increasing the electron density increases the separation between the shifted peaks due to the increase in the frequency of the electron-plasma waves and an electron density of 1.8×10^{18} cm^{-3} is determined from the best fit to the data. The spectra calculated when increasing and decreasing the density by 10% clearly lie outside of the measurement. In the non-collective regime, Figure 6(b) shows that the shape of the spectrum is less sensitive to the density and typically the total scattered power is used when a calibrated collection system is available.

The electron temperature is measured from the shape of the scattering spectrum. Figure 6(c) and (d) show that increasing the electron temperature increases the width of the measured signal. In the collective regime, this is a result of the increased electron Landau damping while in the non-collective regime, this is a result of a broader electron distribution function.

In the collective regime, the calculated spectrum is unique; changing the temperature and the density simultaneously does not reproduce a given spectrum. The uncertainty in the measurement of electron density and temperature is determined by how much n_e and T_e can be varied before the fit falls outside the noise. The uncertainty in the temperature (density) measurement was 5% (10%) in the collective regime. In the non-collective regime the electron density uncertainty from the shape of the spectrum is $\sim 30\%$ and the electron temperature uncertainty is $\sim 25\%$.

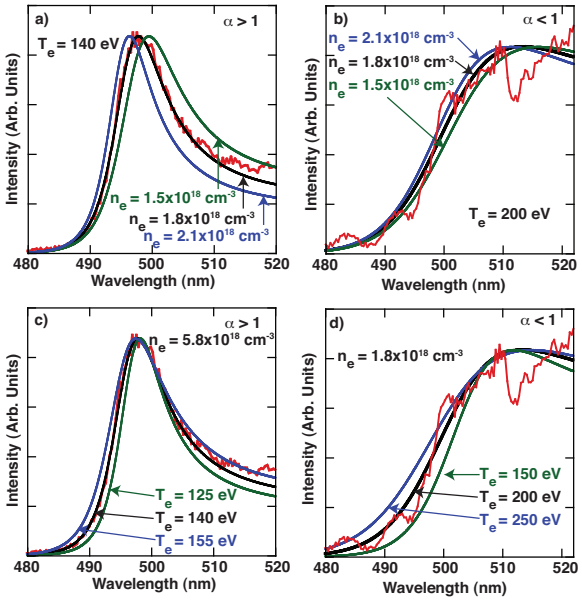

FIG. 6: By varying the electron temperature and density the error in the measurement can be assessed. The experimental data is shown in red and the best fit for each spectra is shown in black: $T_e = 140$ eV, $n_e = 5.8 \times 10^{18}$ cm^{-3} for (a) and (c), $T_e = 200$ eV, $n_e = 1.8 \times 10^{18}$ cm^{-3} for (b) and (d). In plot (a) n_e is increased by 15% for the blue curve and decreased by 15% for the green curve, $T_e = 140$ eV is held constant. In plot (b) n_e is increased by 15% for the blue curve and decreased by 15% for the green curve, $T_e = 200$ eV is held constant. In plot (c) $n_e = 5.8 \times 10^{18}$ cm^{-3} is held constant and T_e is increased by 10% for the blue curve and decreased by 10% for the green curve. In plot (c) $n_e = 1.8 \times 10^{18}$ cm^{-3} is held constant and T_e is increased by 25% for the blue curve and decreased by 25% for the green curve. The actual errors in the measurement of T_e and n_e is clearly less than the ranges shown here.

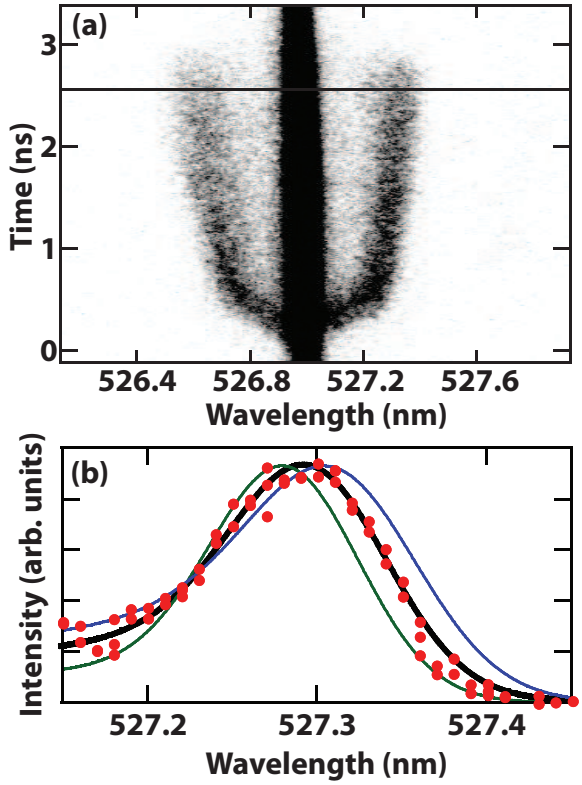

FIG. 7: (a) A streak camera record of the Thomson scattering from the ion feature is shown. The spectra at 2.5 ns is plotted in (b) where the best fit is shown using the electron temperature and density from the simultaneously measured electron feature ($T_e = 240$ eV, $n_e = 1.3 \times 10^{19}$ cm^{-3}). The ion temperature is then varied to fit the ion feature spectra. The best fit is calculated for $T_i = 180$ eV. To assess the error in the ion temperature the spectra is calculated for T_i plus (blue line) and minus (green line) 60 eV.

B. Scattering from low-frequency fluctuations

When $\alpha \gtrsim (ZT_e/3T_i - 1)^{-1/2}$, ion-acoustic features can be observed in the scattering spectrum. The wavelength separation between the two ion-acoustic features ($\Delta\lambda_{IAW}$) is approximately,

$$\frac{\Delta\lambda_{IAW}}{\lambda_i} \cong \frac{4}{c}\sin\left(\frac{\theta}{2}\right)\sqrt{\frac{T_e}{M}\left(\frac{Z}{1+k^2\lambda_D^2}+3\frac{T_i}{T_e}\right)} \quad (7)$$

where M is the ion mass and T_i is the ion temperature. From here it is evident that when ZT_e is on the order of $3T_i$, the frequency of the ion-acoustic features are sensitive to the ion temperature and if ZT_e is known, a measure of T_i can be made.

Figure 7 shows collective scattering from ion-acoustic waves. The measured spectrum 2.5 ns after the rise of the heater beam is compared to the calculated spectrum [Fig. 7(b)]. Using an electron temperature of $T_e = 240$ eV and a density of $n_e = 1.3 \times 10^{19}$ cm^{-3} measured by the associated high-frequency spectrum an ion temperature of $T_i = 180$ eV is measured from the ion spectrum. The average ionization state of $Z = 7$ is calculated using a Thomas-Fermi [17]. The calculated spectra are outside of the measured spectrum when increasing or decreasing the ion temperature by 60 eV while keeping the other parameters fixed demonstrating the sensitivity of the ion feature to the ion temperature. The width of the ion feature is also a function of the ion temperature, but in laser produced plasmas the width is typically dominated by velocity and temperature gradients within the Thomson scattering volume and therefore is an un-reliable measurement of the ion temperature. When multiple ion species can be added to the plasma, an ion temperature measurement can be accurately made by resolving the relative scattered power into each ion acoustic resonance [4, 18].

IV. RESULTS

Thomson scattering measurements are used to measure the hydrodynamic plasma parameters for nitrogen gas jet plasmas with two laser beam configurations. Figure 8 shows the electron temperature and density measurements when the plasma is heated by a 1 ns long pulse (Configuration A). The measurements shows a rapid increase in the electron temperature and density during the initial 200 ps of ionizing the nitrogen gas. As the temperature increases, the rate of inverse bremsstrahlung decreases, and at a temperature of 135 eV and a density of $n_e = 6.0 \times 10^{18}$ cm^{-3} the heating due to inverse bremsstrahlung balances the energy loss due to radiation and expansion and the system is nearly isothermal for the remaining 700 ps of the primary beam. The decrease in the density is linear after initial ionization which is consistent with the plasma expanding into vacuum at the sound speed. The plasma begins to cool at the termination of the primary beam (1 ns). The density decreases to $n_e = 3.0 \times 10^{18}$ cm^{-3} and the temperature to 30 eV by the end of the probe beam (5 ns). At 5 ns the 200 ps high intensity picket reheats the plasma causing an increase in temperature to 80 eV. The density continues to decrease during the picket to a final measured density of $n_e = 2.8 \times 10^{18}$ cm^{-3}. The density decrease is due primarily to the expansion of the plasma and not recombination as is evident by the lack of a density increase when the plasma is reheated.

Figure 9 shows the hydrodynamic parameters as a function of time when the plasma is heated by a 3 ns long beam (Configuration B). The electron temperature and density is determined from the high-frequency Thomson scattering spectrum and the average charge state is calculated to be $Z = 7$. The ion temperautre is then determined. The ion temperature is measured equilibrate with the electron temperature over nearly 3 ns while the density remains constant within the error of the measurement. There error in the ion temperature is determined from both the error in the electron temperature (δT_e) and the error in the separation between the ion-acoustic features ($\delta\Delta_{IAW}$). The absolute error in the ion temperature is,

$$\delta T_i = \left(\frac{\Delta\lambda}{\lambda_i}\right)^2 \left(\frac{c^2 M}{24\sin^2(\theta/2)}\right)\frac{\delta\Delta\lambda}{\Delta\lambda} + \frac{ZT_e}{3\left(1+k^2\lambda_D^2\right)}\frac{\delta T_e}{T_e} \tag{8}$$

derived from Eq. (7). The error in the electron temperature is better than 5% and the error in $\Delta\lambda_{IAW}$ is $\sim 2.5\%$. This results in an error in T_i of 46 to 53 eV for the measurements shown in Fig. 9.

V. SUMMARY

The electron density, and ion and electron temperatures are simultaneously measured in a nitrogen gas jet plasma by collecting Thomson scattered light and spectrally resolving both the electron and ion features. The transition from the non-collective to collective high-frequency regime is observed by varying the electron density. Furthermore, experiments performed in the high-densities typically found in laser produced plasmas result in scattering from electrons moving near the phase velocity of the relativistic plasma waves. Therefore, it is shown that even at low temperatures, relativistic corrections to the scattered power must be included.

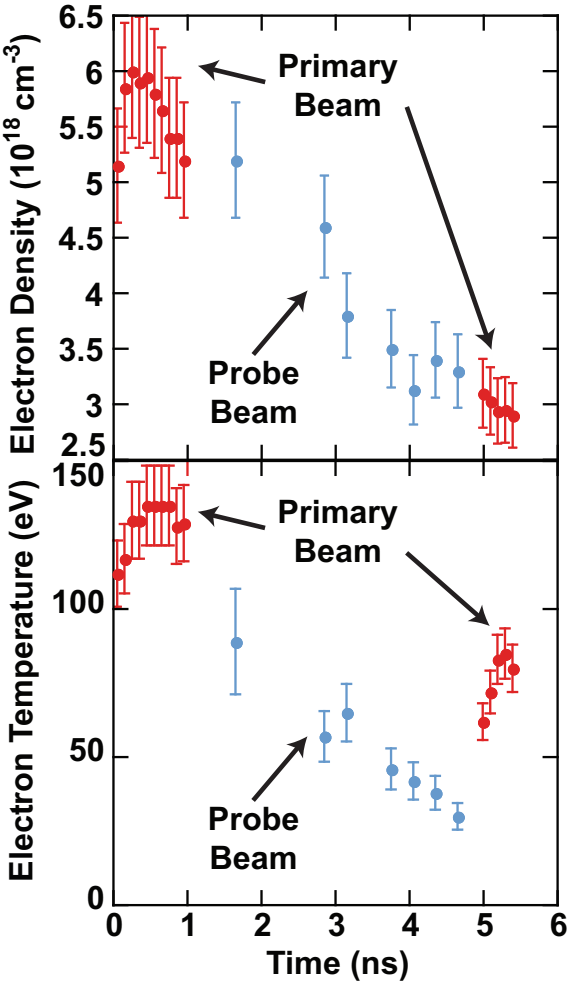

FIG. 8: The electron temperature and density were measured as a function of time. The red points show data measured from the primary beam and the blue points are measured from the probe beam.

VI. ACKNOWLEDGMENTS

This work was performed under the auspices of the U.S. Department of Energy by the Lawrence Livermore National Laboratory under Contract No. DE-AC52-07NA27344.

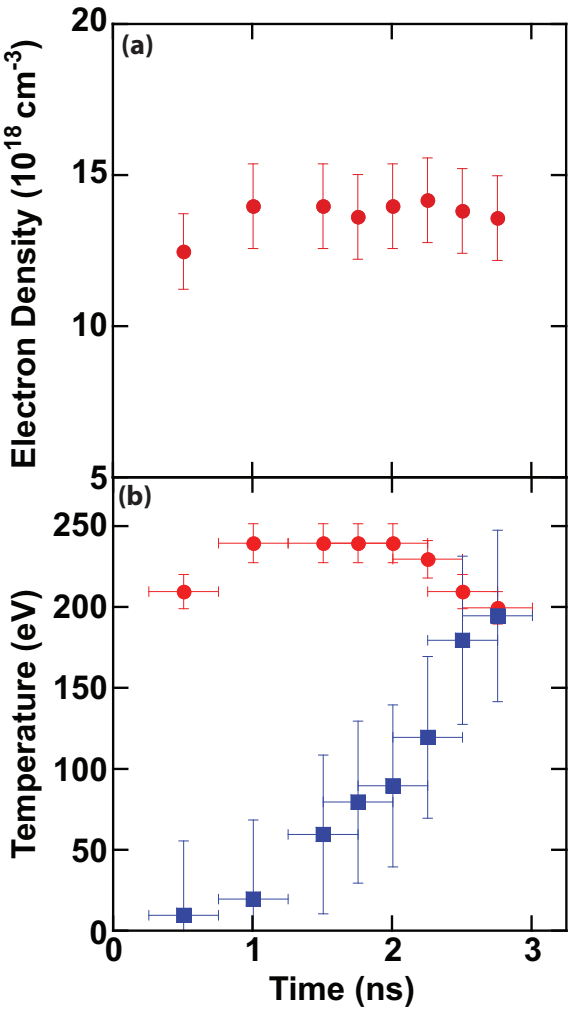

FIG. 9: The electron density (a) and temperature (b) are shown as red circles measured using electron feature using Configuration B. The ion temperature (b) is shown as blue squares measured using the ion feature.

[1] D. H. Froula, L. Divol, and S. H. Glenzer, Physical Review Letters **88**, 105003 (2002).

[2] J. Kline, D. Montgomery, B. Bezzerides, J. Cobble, D. Dubois, R. Johnson, H. Rose, L. Yin, and H. Vu, Phys Rev Lett **94**, 175003 (2005).

[3] D. Montgomery, J. Kline, and T. Tierney, *Detailed characterization of plasma wave behavior using collective thomson scattering (invited)* (2004).

[4] S. H. Glenzer, C. A. Back, K. G. Estabrook, R. Wallace, K. Baker, B. J. MacGowan, B. A. Hammel, R. E. Cid, and J. S. De Groot, Physical Review Letters **77**, 1496 (1996).

[5] N. Peacock, D. Robinson, M. Forrest, P. Wilcock, and V. Sannikov, Nature **224**, 488 (1969).

[6] R. Behn, D. Dicken, J. Hackmann, S. Salito, M. Siegrist, P. Krug, I. Kjelberg, B. Duval, B. Joye, and A. Pochelon, Phys Rev Lett **62**, 2833 (1989).

[7] F. Alladio and M. Martone, Phys Lett A **60**, 39 (1977).

[8] T. Wrubel, S. Buscher, and H. Kunze, Plasma Phys Contr F **42**, 519 (2000).

[9] R. Pasqualotto, A. Sardella, A. Intravaia, and L. Marrelli, Rev Sci Instrum **70**, 1416 (1999).

[10] S. H. Glenzer, L. M. Divol, R. L. Berger, C. Geddes, R. K. Kirkwood, J. Moody, E. A. Williams, and P. E. Young, Physical Review Letters **86**, 2565 (2001).

[11] D. H. Froula, L. Divol, D. G. Braun, B. I. Cohen, G. Gregori, A. Mackinnon, E. A. Williams, S. H. Glenzer, H. A. Baldis, D. S. Montgomery, et al., Physics of Plasmas **10**, 1846 (2003).

[12] S. H. Glenzer, W. Rozmus, B. J. MacGowan, K. G. Estabrook, J. D. De Groot, G. B. Zimmerman, H. A. Baldis, J. A. Harte, R. W. Lee, E. A. Williams, et al., Physical Review Letters **82**, 97 (1999).

[13] J. S. Ross, S. H. Glenzer, J. P. Palastro, B. B. Pollock,

D. Price, L. Divol, G. R. Tynan, and D. H. Froula, Phys Rev Lett **104**, 105001 (2010).
[14] S. Dixit, M. Feit, M. Perry, and H. Powell, Optics Letters **21**, 1715 (1996).
[15] A. Visco, R. P. Drake, D. H. Froula, S. H. Glenzer, and B. B. Pollock (AIP, 2008), vol. 79, p. 10F545.
[16] J. Sheffield, *Plasma Scattering of Electromagnetic Radiation* (Academic, New York, 1975).
[17] D. Salzmann, *Atomic Processes in Hot Plasmas* (Oxford University Press, Oxford, U.K., 1998).
[18] D. Froula, L. Divol, and S. Glenzer, Phys Rev Lett **88**, 105003 (2002).